PCCP

Accepted Manuscript

ROYAL SOCIETY OF CHEMISTRY

www.rsc.org/pccp

Cite this: DOI: 10.1039/c0xx00000x

www.rsc.org/xxxxxx

ARTICLE TYPE

Enhanced Charge Collection with Ultrathin AlO_x Electron Blocking Layer for Hole-Transporting Material-Free Perovskite Solar Cell

Huiyun Wei,[a] Jiangjian Shi,[a] Xin Xu,[a] Junyan Xiao,[a] Jianheng Luo,[a] Juan Dong,[a] Songtao Lv,[a] Lifeng Zhu,[a] Huijue Wu,[a] Dongmei Li,[a] Yanhong Luo[a], Qingbo Meng,[a]* and Qiang Chen[b]*

Received (in XXX, XXX) XthXXXXXXXXX 20XX, Accepted Xth XXXXXXXXX 20XX
DOI: 10.1039/b000000x

Ultrathin AlO_x layer has been deposited onto the $CH_3NH_3PbI_3$ film by atomic layer deposition technology, constructing a metal-insulator-semiconductor (MIS) back contact for the hole-transporting-material-free perovskite solar cell. By optimization the ALD deposition cycles, average power conversion efficiency (PCE) of the cell has been enhanced from 8.61% to 10.07% with the highest PCE of 11.10%. It is revealed that the improvement in cell performance with this MIS back contact is mainly attributed to the enhancement in charge collection resulting from electron blocking effect of the AlO_x layer.

1. Introduction

Organolead halide perovskites have shown great potential as light harvesters for solar cells due to their superb optical and electric properties.[1,2]From the liquid-type to solid-state,[3,4] the perovskite solar cell (PSC) had experienced a rapid development in short five years, and power conversion efficiencies (PCE) over 17% have been achieved.[5-8]Currently, highly efficient PSCs are all based on the hole transporting material (HTM), which can facilitate the hole transport and collection and block the electron transfer. In view of decreasing cost and simplifying the cell structure, HTM-free PSCs have also been developed[9-12].With Au electrode, the PCE of the cell has been promoted exceeding 10% with effort on the perovskite film deposition[10-12].Meanwhile, the carbon electrode has also been introduced to enhance the charge collection and transport at the back contact, and a high PCE of 12.8% was achieved.[13,14]Promising prospect has been shown for the HTM-free PSC, however, the PCE of the cell needs to be further improved to really make a competition with the HTM based cell and the mature solar cells.

To the HTM-free PSCs, besides depositing high-quality perovskite films, interface engineering and design are also effective approaches to enhance the device performance by improving the charge collection and suppressing surface recombination.[8,13,14]According to our previous works, photo-induced carriers at back contact region cannot be efficiently collected in the HTM-free PSC without effective back surface filed (BSF).[10,15,16] Without the HTM, semiconductor $CH_3NH_3PbI_3$ may contact directly with Au electrode, forming a metal-semiconductor (M-S) interface. For an unmodified M-S interface, series charge recombination can occur due to interfacial defects.[17] Meanwhile, photo-induced free electrons may also transfer into the metal electrode because the minor carrier diffusion length is comparable and even larger than the thickness of the absorber in the perovskite solar cell. Moreover, an energy barrier for hole transport usually exists at this M-S interface due to a low Fermi energy level in $CH_3NH_3PbI_3$.[10]Thus, to the HTM-free PSCs, back contact and recombination are likewise the key barriers to improve the cell performance.[10,11,15] To avoid the negative influence mentioned above, some modifications toward the M-S interface have been carried out. For example, the small organic molecule with wide bandgap, TPB(N,N,N',N'-tetraphenyl-benzidine was introduced to the perovskite interface to enhance the PCEs of HTM-free PSCs.[16] Recently, Snaith and his colleagues have also made a modification on perovskite/HTM interface with organic iodopentafluorobenzene (IPFB) and achieved a stable output PCE of 15% [18] . Besides organic molecules, inorganic compounds, such as Al_2O_3, MgO, MoO_3, can also effectively modify the interfaces between semiconductors and metal electrode or liquid electrolyte.[15,19-22] Introduction of ultrathin insulator Al_2O_3 film into $CH_3NH_3PbI_3$/Au interface has been proved to be effective on the cell performance in our lab.[15]In this respect, the influence of ultrathin AlO_x film thickness on the metal-insulator-semiconductor (MIS) back contact for the perovskite cell has been further investigated. Meanwhile, the working mechanism of this MIS back contact has been first systematically clarified. With this MIS back contact, the internal quantum efficiency (IQE) of the cell in the long wavelength region is enhanced significantly, leading to the increase in photocurrent. It is revealed that different ALD deposition cycles have remarkably influenced on interfacial carrier transfer and 5 cycles ALD of AlO_x can exhibit the best cell performance. Finally, the average PCE of the HTM-free PSC with Au electrode has been enhanced from 8.61% to 10.07%, and a PCE exceeding 11% has also been firstly achieved with this interfacial modification. X-ray photoelectron spectroscopy (XPS), incident photon-to-electron conversion efficiency (IPCE), impedance spectra (IS), transient photoluminescence (PL) and photovoltage, and analysis based on semiconductor physics have been employed to clarify the

influence of this MIS back contact and mechanism behind this enhancement in PCE. It is revealed that the ultrathin AlO_x can act as an effective electron blocking layer to enhance charge collection in this HTM-free cell.

2. Experimental section

Materials

PbI_2 (99%) and dimethylformide (DMF, 99.7%) were purchased from Aldrich and Alfar Aesar, respectively. CH_3NH_3I was synthesized as literature described. Fluorine-doped tin oxide conducting glass (FTO, Pilkington, thickness 2.2 mm, sheet resistance 14 Ω/ square) was used as substrates for the solar cell. Before use, FTO glass was first washed with mild detergent, rinsed with distilled water for several times and subsequently with ethanol in an ultrasonic bath, finally dried under air stream. AlO_x films were deposited with $Al(CH_3)_3$ [trimethylauminum (TMA)] and H_2O as the precursors. The carrier gas in the viscous flow reactor was N_2 (ultrahigh purity).

Fabrication of the device

All the experiments were carried out in ambient condition with the humidity of about 25%. The compact TiO_2 layer was spin-coating on the FTO and heated at 500 ℃ for 30 min. The mesoporous TiO_2 layer composed of 20-nm-sized particles was subsequently deposited by using screen-printing technique, which was first dried at 80 ℃ for 30 min, and then sintered at 500 ℃ for 30 min. Afterwards, the films were immersed into 25 mM $TiCl_4$ at 70 ℃ for 40 min and then sintered at 500 ℃ for 30 min.

The $CH_3NH_3PbI_3$layer was deposited by a modified two-step deposition method as described previously.[10] Firstly, the solution of 1.2 M PbI_2 dissolved in DMF was spin-coated onto TiO_2 film at a speed of 2000 rpm for 60 s, and then heated at 90 ℃ for 2 min to remove the DMF solvent. After cooling to room temperature, the film was spin coated with the PbI_2 solution for a second time to increase the amount of PbI_2 and get a relatively smooth film. After dried at 90 ℃ for another 2 min and cooling down, the films were immersed in a solution of CH_3NH_3I (10 mg/mL) with 2-propanol as the solvent for 120 min, and rinsed with 2-propanol thoroughly. Finally, the $TiO_2/CH_3NH_3PbI_3$ film was heated at 90 ℃ for 45 min in air on a hotplate.

ALD of AlO_x

The ultrathin AlO_x insulating layer was deposited onto $CH_3NH_3PbI_3$ film by ALD technology in a viscous-flow ALD reactor, which has been described in other publications.[23,24]Briefly, TMA and H_2O were used as precursor gases, and high-purity N_2 was used as carrier gas for the precursors. TMA and H_2O were alternately entrained in the N_2 carrier flow using gas switching valves, and the N_2 carrier gas pressure was about 0.1 Torr. The deposition temperature was kept at 100 ℃ over the entire deposition process to obtain high quality AlO_x films. During the deposition process, for per cycle, the exposure time of TMA and H_2O were set as 0.3s and 0.05s, respectively, and the pumping gas time of 10s and 30s were separately required for purging the excess TMA and H_2O. Varied ALD cycles have been carried out to deposit the AlO_x ultrathin film. For comparison, a batch of control samples which were put in the reactor chamber (0.1 Torr, 100 ℃, N_2 flow) without any precursor have also been prepared.

Characterization of the solar cell

The surface morphology of the FTO/TiO_2/ $CH_3NH_3PbI_3$ film was characterized by using a scanning electron microscope (SEM, FEI XL30S-FEG). The X-ray photoelectron spectroscopy (XPS) data was obtained using an ESCALab250 electron spectrometer from Thermo Scientific Corporation with monochromatic 150 W Al Kα radiation. The current-voltage (*I-V*) performance of the cells was measured by an additional voltage from the 2602 system source meter of Keithley together with a sunlight simulator (Oriel Solar Simulator 91192, AM 1.5 100mW/cm^2) calibrated with a standard silicon reference cell. The solar cells were masked with a black aperture to define the active area of 0.08 cm^2 and measured in a lab-made light-tight sample holder. The current of the cell is recorded every 5 mV with a delay time of 0.1 s for each step, which is approximately equal to a scan rate of 50 mV/s. Monochromatic incident photo-to-electron conversion efficiency (IPCE) was measured with a lab-made IPCE spectrometer[25,26] with wavelength ranging from 350 nm to 850 nm. UV-Vis absorption and transmittance spectrum was measured with UV-Vis spectrophotometer (UV-2550, SHIMADZU) with wavelength ranging from 350 nm to 850 nm. Impedance spectra (IS) for the solar cell was measured on a ZAHNER IM6e electrochemical workstation in dark with the frequency ranging from 0.1 to 10^5 Hz and a perturbation amplitude of 10 mV. Transient photoluminescence (PL) spectra was obtained on a PL Spectrometer (Edinburgh Instruments, FLS 900), and excited with a picosecond pulsed diode laser (EPL-445, 0.8 μJ/cm^2, 1 MHz) at 445 nm. Transient photovoltage was measured with a pulsed Nd:YAG laser (Brio, 20 Hz) at 532 nm and a nanosecond resolved digital oscilloscope (Tektronix DPO 7104).

3. Results and discussion

The scheme of $CH_3NH_3PbI_3/TiO_2$heterojunction solar cell with the MIS back contact is depicted in Figure 1(a), where an ultrathin AlO_x insulating layer was introduced between $CH_3NH_3PbI_3$ and Au to avoid their direct contact. The cross-sectional scanning electron microscope (SEM) image of the cell without Au electrode is shown in Figure 1(b). The mesoporous TiO_2 film with a thickness of about 500 nm can be clearly seen, where the pores have been completely infiltrated with the $CH_3NH_3PbI_3$ crystals. Over the TiO_2 layer, a dense $CH_3NH_3PbI_3$ capping layer with a thickness of about 300 nm can also be clearly seen. Moreover, with the SEM image, it can be seen that $CH_3NH_3PbI_3$ crystals inside the TiO_2 pores and in the capping layer connect tightly with each other, benefitting for charge transport throughout the cell. It is worth noting that due to the dense $CH_3NH_3PbI_3$ capping layer and a complete infiltration inside TiO_2 pores, the diffusion of CH_3NH_3I inside the TiO_2 layer is ultra-slow at room temperature, leading to a long immersion time for completely converting PbI_2 into $CH_3NH_3PbI_3$ in our experiment. Although an AlO_x layer has been deposited onto the $CH_3NH_3PbI_3$ film, it is too thin to be observed in this SEM image. To check whether the AlO_x had been successfully

deposited with five ALD cycles, XPS was applied to investigate the elemental composition of the film. Figure 2(a) gives the full XPS spectra of $TiO_2/CH_3NH_3PbI_3/AlO_x$ film with binding energy ranging from 0 to 1200 eV. The Al *2p* peak locating at 75.18 eV is shown Figure 2(b), implying the existence of aluminum on the $CH_3NH_3PbI_3$film. However, the peak was slightly shifted towards a higher binding energy compared to that in stoichiometric Al_2O_3 of 74.60 eV.[27] Thus, the aluminum coating on the perovskite film is more like in a form of AlO_x. Meanwhile, an interaction between aluminum and the under-coordinated iodide may also influence the binding energy of Al *2p*.

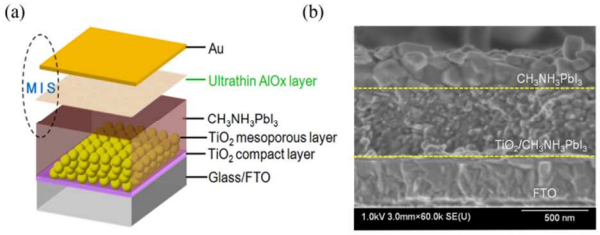

Figure 1 (a) The scheme of $CH_3NH_3PbI_3/TiO_2$heterojunction solar cell with the MIS back contact; (b) Cross-sectional scanning electronic microscope image of the FTO/TiO_2/ $CH_3NH_3PbI_3/AlO_x$ film.

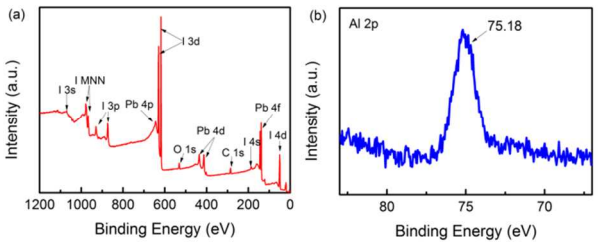

Figure 2 (a) XPS spectra of the $CH_3NH_3PbI_3$with five-ALD-cycles. (b) XPS spectra of Al *2p*.

The photocurrent density-voltage (*J-V*) characteristics of the cells where AlO_x was deposited onto the $CH_3NH_3PbI_3$ film for varied ALD cycles are shown in Figure 3. For ALD-1 cells (not shown), no *J-V* difference can be observed from the ALD-0 cells, implying little AlO_x has been deposited on the perovskite film only for one cycle in our deposition condition. Further increasing the ALD cycles from zero to five, the photovoltaic performance of the cell has been significantly improved with enhancement in short-circuit current density (J_{SC}) and open-circuit voltage (V_{OC}), as shown in Figure 3(a). However, when AlO_x was deposited for six and seven cycles, significant decrease in V_{OC} and fill factor (*FF*) of the cell can be observed. For the *J-V* characteristics of ALD-6 (and 7) cells, a slight bend near V_{OC} can be observed, as shown in Figure 3(b), indicating an S-shaped feature. It thus can be inferred that the holes are blocked when transporting from $CH_3NH_3PbI_3$ to Au electrode due to the relatively thick AlO_x insulating layer.[28] The statistic results of J_{SC}, V_{OC}, *FF* and PCE from a batch of ninety solar cells are given in Figure 4(a)-(d), respectively. For ALD-0 cells, the average PCE is about 8.61% with average J_{SC} of 15.02 mA/cm^2, V_{OC} of 885 mV, *FF* of 0.643. After ALD-AlO_x treatment of $TiO_2/CH_3NH_3PbI_3$ film, the average PCE is enhanced to 10.07% with average J_{SC} of 17.10 mA/cm^2, average V_{OC} of 918 mV and average *FF* of 0.643. It can be clearly seen that the enhancement in J_{SC} makes more contribution to the improvement of PCE. With this ALD modification on M-S back contact, the highest efficiency of the cell is promoted to 11.10% with J_{SC} of 17.62 mA/cm^2, V_{OC} of 921 mV and *FF* of 0.684, as shown in Figure 5(a). Integral current density from the IPCE (Figure 5(b)) of this cell can obtain 16.56 mA/cm^2, basically in agreement with the *J-V* result. To investigate whether the ALD condition but not the deposited AlO_x layer contributes to the enhancement in cell performance, a group of cells which were put in the ALD chamber (0.1 Torr, 100 °C, N_2 flow) for the same time with ALD-5 samples without any release of the precursors were prepared. It has been found that the cell performance cannot be improved just with the ALD condition, but slightly decreased as in Figure S1. It is also worth noting that the *J-V* hysteresis has not been enhanced with the AlO_x deposition, as shown in Table S1, which implies that the improvement of cell performance cannot be due to carrier accumulation and capacitance effect coming from swept measurement.[29] Therefore, the introduction of AlO_x layer can indeed improve the cell performance, especially increase the J_{SC}. To investigate the working mechanism of this MIS back contact, analysis based on IPCE, IS, PL and photovoltage, and theory of semiconductor physics will be made in the following section.

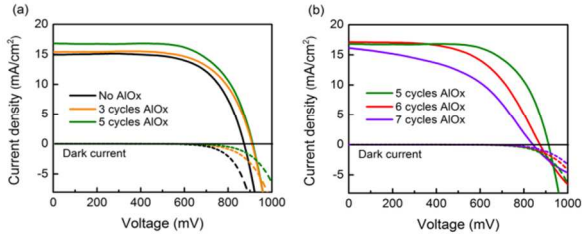

Figure 3 Photocurrent-voltage (*J-V*) characteristics for the perovskite solar cells with 0, 3, 5, 6 and 7 ALD cycles, respectively. Solid and dashed lines correspond to measurements under simulated AM 1.5G solar irradiance (100 mW/cm^2) and in the dark, respectively.

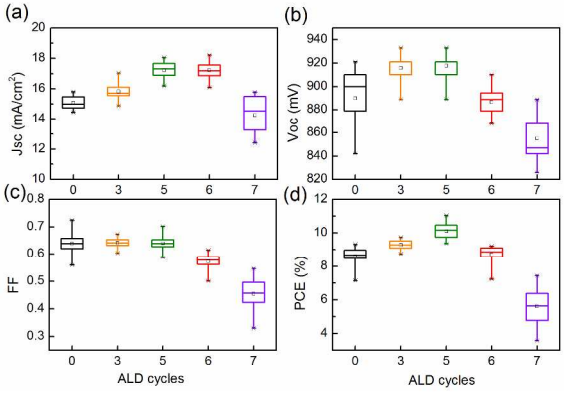

Figure 4 Photovoltaic parameters of (a) J_{SC}, (b) V_{OC}, (c) *FF* and (d) PCE extracted from current-voltage measurements of the solar cells without and with different AlO_x ALD cycles. The horizontal axis represents the number of AlO_x ALD cycles.

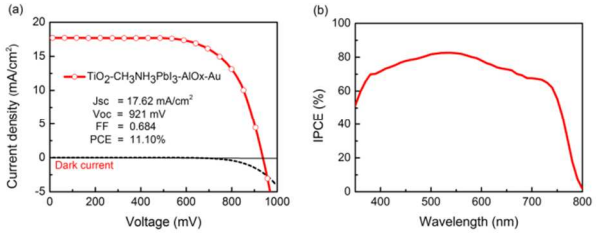

Figure 5 (a) The *J-V* characteristics for highest efficiency perovskite solar cell with five ALD cycles. (b) The IPCE of the perovskite solar cell.

The IPCE spectra of the cells in Figure 3 is given in Figure 6(a) and light harvesting efficiency (LHE) of the cell is given in Figure S2. For ALD-3 cell, IPCE in the long-wavelength region is enhanced compared to the ALD-0 cell, which implies that the charge generated close to back contact of the cell can be collected more effectively.[30] For ALD-5 cell, IPCE in the whole visible wavelength region is enhanced, thus leading to a significant improvement of J_{SC}. IPCE is not just an assisting measurement for accurately determine the J_{SC}, but also effective for investigation in charge generation, transport and collection of a cell. The mechanism of charge loss in a cell can also be studied with IPCE.[30]For a single-heterojunction cell without BSF, a serious charge transfer from semiconductor absorber layer to back electrode as well as serious minor carrier recombination usually exist, decreasing the charge collection in the deep region of a cell (IPCE in long-wavelength region). An effective BSF is one of the key factors for the high-efficiency solar cells such as Si and Cu(In, Ga)Se_2 cells.[31,32] However, different from HTM-based cell, no BSF has been applied into the HTM-free perovskite solar cell. Thus, IPCE in the long wavelength region is usually much lower than that in short wavelength region, as in Figure 6(a). Interestingly, with the MIS back contact, charge collection in deep region of the cell has been significantly increased, as shown with the normalized IPCE in Figure 6(b). Thus, electron transfer from $CH_3NH_3PbI_3$ to Au electrode or charge recombination has been suppressed with the MIS back contact. To clarify what makes more contribution to the enhancement in charge collection and thus the cell performance, transient PL, photovoltage and IS measurements have been carried out.

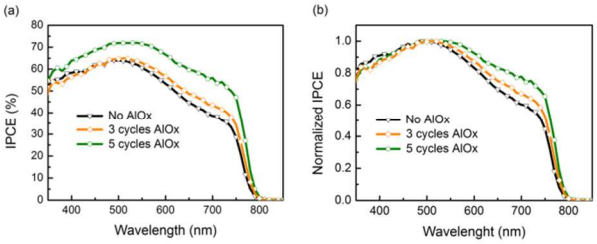

Figure 6 (a) IPCE of the perovskite solar cells with 0, 3, 5 ALD cycles, respectively. (b) The Normalized IPCE of the solar cells.

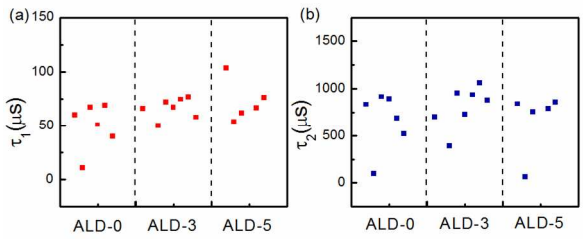

Figure 7 The recombination lifetimes of carriers in the HTM-free solar cells with or without the AlO_x layer, which were obtained by biexponential fitting of transient photovoltage. (a) The short lifetime of about 50μs. (b) The long lifetime of about 1000 μs.

Transient PL is applied to investigate charge recombination of $CH_3NH_3PbI_3$ film and several groups of samples have been measured to get a reliable average PL lifetime. Double exponential function was used to fitting the PL results and the longer lifetime is listed in Table 1. It can be found that no influence on the PL lifetime of $CH_3NH_3PbI_3$ film has been brought with introduction of the AlO_x layer. Thus, it can be inferred that the charge recombination in back contact region has not been suppressed with this MIS back contact. To confirm this speculation, transient photovoltage of the cells has also been measured, fitting results with double exponents of which are shown in Figure 7 with short lifetime (a) of about 50 μs and long lifetime (b) of about 1000 μs. No difference in the recombination lifetime of the cell can be distinguished from the transient photovoltage measurement. Therefore, it can be concluded that the enhancement in cell performance mainly comes from the suppression on electron transfer from $CH_3NH_3PbI_3$ to Au electrode with the MIS back contact.

Table 1 PL lifetime of solar cells with 0, 3, 5 ALD cycles, respectively.

Cell	PL lifetime (ns)				
	1	2	3	4	Average value
ALD-0	176.69	173.04	153.39	162.43	166.39
ALD-3	159.68	166.10	165.24	155.07	161.52
ALD-5	164.27	154.56	162.30	176.14	164.32

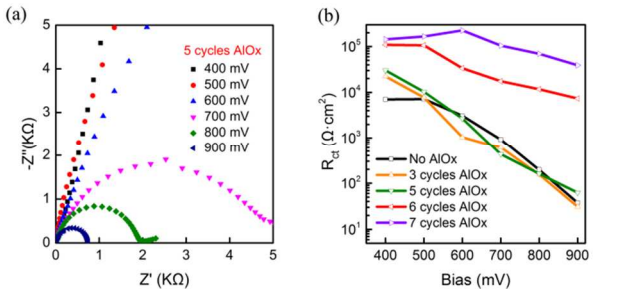

Figure 8 (a) Nyquist plots of the ALD-5 perovskite solar cell under dark. (b) Plots of charge transfer resistance (Rct) for perovskite solar cells with different ALD cycles at various bias voltages.

IS is an effective measurement on charge transfer properties of a cell and has been widely used in study of PSCs.[33-36] Figure 8(a) gives the Nyquist plots of ALD-5 cell and the fitting results from the IS results with one RC element as the equivalent circuit. In the frequency ranging from 10^5 Hz to 0.1 Hz, one typical

semicircle can be distinguished from the Nyquist plots, which can be assigned to $TiO_2/CH_3NH_3PbI_3$ interface.[30] Interestingly, no difference in charge transfer resistance (Rct) can be found, either, from the fitting results for ALD-0 to ALD-5 cells, as in Figure 8(b), which implies that the MIS back contact with an ultrathin AlO_x layer has not influenced the charge transfer properties at $TiO_2/CH_3NH_3PbI_3$ interface. However, a significant increase in Rct appears when the AlO_x layer is becoming thicker, which seems to conflict with the *J-V* results if just considering an ideal model. [37] In nanometer-scale semiconductor devices, the interfaces can usually be coupled together if severe charge accumulation occurs and the IS can hardly give accurate information on interfacial charge transfer. Although the working mechanism of the MIS back contact in this cell cannot be clearly clarified with IS results, the sudden increase in Rct for ALD-6 and ALD-7 cells implies a voltage sharing effect in this cell. Thus, the *J-V* characteristics of the cells will be analyzed in detail in following.

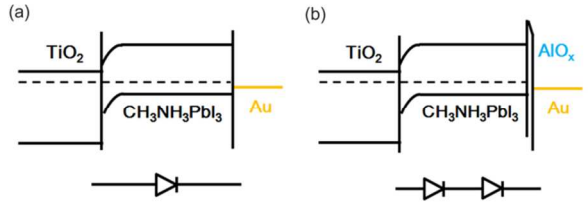

Figure 9 (a) Energy band structure of the solar cells without AlO_x layer. (b) Energy band structure of the solar cells with an ultrathin AlO_x layer.

For the HTM-free PSC, a single heterojunction model can be employed to describe the charge transfer property of the cell.[11] With this ideal model as depicted in Figure 9(a), the *J-V* characteristics in dark can be written as[38]

$$J = -J_0 \times \left[\exp\left(\frac{e(V + J \times R_S)}{AK_BT} \right) - 1 \right] \quad (1)$$

Where J_0 is the inverse saturated current density of the heterojunction, R_S is the series resistance, A is the ideality factor of a single heterojunction ranging from 1 to 2, K_B is the Boltzmann constant, and T is the absolute temperature. With this equation and *J-V* results of the cells in dark (Figure 3), the intrinsic parameters of this heterojunction cell are deduced, as given in Table 2. The cell without AlO_x deposition shows a normal ideality factor of 2.02 with a small R_S of 1.42 Ω cm^2 and a relatively small J_0 of 3.09×10-6 mA/cm^2, agreeing with the published results and the ideal model.[10,15] For ALD cells, the R_S increases gradually as expected due to adding of the insulating AlO_x layer. Meanwhile, the J_0 has also been slightly changed. Interestingly, the ideality factor has a significant change from 2.02 to about 2.63, beyond the range of a single heterojunction, indicating a series connection of two or more diodes. For example, the ideality factor of a multijunction GaAs solar cell is 3.27, much larger than that of the single junction GaAs cell (1.51).[39,40]Considering the MIS structure, a new diode can appear in the cell, as depicted in Figure 9(b). For an MIS tunneling diode, the current characteristics can also be described with equ. (1). Thus, when taking the charge transfer through both the photoanode and the back contact into consideration, the current density-voltage characteristics of the cell in dark can be derived as

$$J \approx J_{10}\left(\frac{J_{20}}{J^{10}}\right)^{A2/(A1+A2)} \times \left[\exp\frac{eV}{(A_1 + A_2)KT} - 1 \right] \quad (2)$$

where the subscript number 1, 2 is assigned to photoanode and back contact, respectively. It can be clearly seen that the ideality factor of the cell can be increased when the charge transfer property is determined by both the $TiO_2/CH_3NH_3PbI_3$ and the $CH_3NH_3PbI_3$/Au interfaces. With equ. (2), the J_{20} of the back contact can also be calculated, which is also listed in Table 2. As can be seen, with the ultrathin AlO_x layer, the electron transfer from $CH_3NH_3PbI_3$ to Au has been significantly suppressed with decreased J_{20} to 10^{-6} mA/cm^2.

In back contact region of the cell without BSF, no depleted electric filed exists for fast extraction of photo-induced electrons and the free electrons are mainly collected with diffusion mechanism.[32]When light coming from the FTO side, carriers in $CH_3NH_3PbI_3$ are induced, transport and collected by electrodes of the cell. In depth x of the $CH_3NH_3PbI_3$ absorber, carrier generation can be described as[32]

$$G(x) = \int_{E>E_g} (1-R)\alpha(E)Q(E)e^{-\alpha x}dE \quad (3)$$

where R is the reflection of the cell, α is light absorption coefficient and Q is the spectral distribution of the sun. It can be demonstrated that charge generation decreases gradually when depth x increases. Thus, a distribution of initial photo-induced electron density (n) in the $CH_3NH_3PbI_3$ layer appears where n decreases as G if the absorber is so thick that the free electrons have to transport for a long length to be collected. Just considering carrier diffusion, electron density and transport in the absorber layer can be described as[32]

$$\begin{cases} \dfrac{\partial n}{\partial t} = \dfrac{1}{q}\dfrac{\partial J_n}{\partial x} + G_n - U_n \\ J_n = qD_n \dfrac{\partial n}{\partial x} \end{cases} \quad (4)$$

Where U_n is carrier recombination velocity, and D_n is electron diffusion coefficient. Obviously, due to decrease in n when x increases, J_n<0, which means that free electrons can diffuse toward the back contact spontaneously. A wide-known steady-state diffusion equation can be deduced from equ. (4) and electron transfer characteristic at back contact determines the boundary condition for this diffusion equation. In a semiconductor, the free electron density can be described as $n=n_0[\exp(eV/K_BT)-1]$, where n_0 is the electron density of thermal equilibration and V is the voltage at this semiconductor. For M-S based perovskite solar cell, no designed BSF exists at back contact, and free electron can transfer toward Au electrode without any blocking. Thus, no voltage can be applied at this M-S interface, and $n_{M\text{-}S}=n_0$. For an interface where electron transfer is limited, voltage sharing effect appears and $n>n_0$, [23] For MIS back

contact, the free electrons diffusing spontaneously toward the back contact can be blocked with the ultrathin AlO_x layer as the J_{20} in Table 2 shows and accumulate at the MIS interface, thus significantly increasing n. Considering the steady-state diffusion equation and the boundary condition for different back contact, the distribution of electron density can be depicted as in Figure 10. It can be seen that with electron blocking, electron density at the back contact interface increases and thus significantly decreases the gradient of electron density. Electron diffusion to the back contact can be significantly suppressed, thus leading to enhancement in charge collection by $TiO_2/CH_3NH_3PbI_3$ interface. We think that this is the mechanism for the MIS back contact in our work. It is worth noting that the MIS back contact can only perform very well in the cell with a thick absorber, as shown in Table S2. Decreasing the thickness of the $CH_3NH_3PbI_3$ absorber, the photo-induced electrons can be more effectively collected by the TiO_2 layer.

Table 2 The intrinsic parameters of the solar cells derived from *J-V* results of the cells in dark.

ALD cycles	R_S (Ω cm^2)	A	J_0 (mA/cm^2)	J_{10} (mA/cm^2)	J_{20} (mA/cm^2)
0	1.42	2.02	3.09×10^{-6}	3.09×10^{-6}	-
3	2.69	2.71	8.10×10^{-6}	3.09×10^{-6}	1.55×10^{-4}
5	13.07	2.58	2.90×10^{-6}	3.09×10^{-6}	2.35×10^{-6}
7	12.31	2.63	2.26×10^{-6}	3.09×10^{-6}	0.85×10^{-6}
Spiro	-	3.1	3.40×10^{-7}	3.09×10^{-6}	6.09×10^{-9}

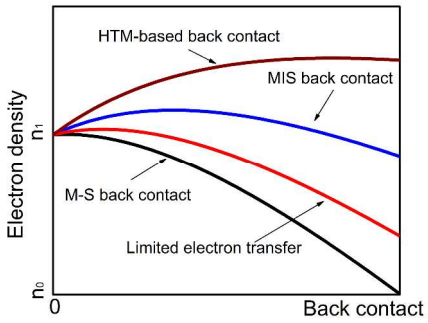

Figure 10 Schematic diagram for the distribution of photo-induced electron in $CH_3NH_3PbI_3$ absorber layer with different back contact.

According to the ideality factors listed in Table 2, the electron blocking effect indeed appears with the MIS back contact. Thus, the improvement of cell performance in our work can be attributed to the suppression of electron transfer from $CH_3NH_3PbI_3$ to Au electrode and enhancement in charge collection with the MIS back contact. For the HTM-based PSC, free electrons can hardly transfer into the HTM due to energy structure and electron state in HTM, leading to a distribution of free electron density as in Figure 10, where the gradient of electron density as well as J_{20}at the perovskite/HTM interface is ultra-small. Meanwhile, photo-induced holes in the perovskite absorber can be fast neutralized with electrons from the HTM. This is one of the key factors for the high efficiency in HTM-based PSC. Dr. Kamat has also calculated the ideality factor of the HTM-based cell,[41] yielding 5.0 for Spiro-OMeTAD and 2.7 for CuI, both of which exceed the ideal range of a single heterojunction and indicating a diode at the perovskite/HTM interface. Thus, a large ideality factor is needed for high efficiency of a cell. Although the MIS back contact with the ultrathin AlO_x layer can increase the ideality factor, $J_0$of the cell has still not been significantly suppressed as in Table 2, which indicates that electron blocking ability of the AlO_x layer is weaker than that of HTM. Meanwhile, the AlO_x layer can also block the electron transfer from Au electrode to the valence band of $CH_3NH_3PbI_3$, decreasing cell performance and causing S-shaped *J-V* feature for ALD-6 and ALD-7 cells. Therefore, we will try to find a low-cost and easy-deposited film which can effectively block electron transfer unidirectionally in our future work.

Conclusions

Ultrathin AlO_x has been deposited onto the $CH_3NH_3PbI_3$ film with ALD technology, constructing an MIS back contact for the HTM-free PSC. With this MIS back contact, average PCE of the cell has been enhanced from 8.61% to 10.07% with the highest PCE of 11.10%. It has been found that charge collection ability of the cell in long-wavelength region is significantly enhanced with this MIS back contact according to IPCE measurements. Charge recombination in $CH_3NH_3PbI_3$ close to back contact has been demonstrated not being influenced with this AlO_x layer according to transient PL and photovoltage measurements. IS and analysis on *J-V* characteristics have been employed to investigate charge transfer properties of the cell. It is thus found that the ultrathin AlO_x can obviously increase the ideality factor of the cell, indicating a diode appearing at the MIS back contact. Therefore, it can be concluded that the AlO_x layer can act as an electron blocking layer to suppress electron transfer from$CH_3NH_3PbI_3$ to Au electrode. It has also been semi-quantitatively demonstrated that this electron blocking effect can enhance charge collection in the cell with considering carrier diffusion in absorber layer. Finally, the improvement in cell performance with the MIS back contact is mainly attributed to the enhancement in charge collection resulting from electron blocking effect of this AlO_x layer.

Acknowledgements

This work was supported by the National Key Basic Research Program (973 project, No. 2012CB932903 and 2012CB932904), Beijing Science and Technology Committee (No.Z131100006013003), NSFC (Nos. 51372270, 51372272, 11474333, 91233202 and 21173260) and the Knowledge Innovation Program of the Chinese Academy of Sciences.

Notes and references

[a] *Key Laboratory for Renewable Energy, Chinese Academy of Sciences; Beijing Key Laboratory for New Energy Materials and Devices; Institute of Physics, Chinese Academy of Sciences, Beijing 100190, P. R. China*

[b] *Laboratory of Plasma Physics and Materials, Beijing Institute of Graphic Communication, Beijing 102600, P. R. China*
** E-mail: qbmeng@iphy.ac.cn, lppmchenqiang@hotmail.com, Fax: +86-10-8264-9242, Tel: +86-10-8264-9242*

† Electronic Supplementary Information (ESI) available:The*J-V* characteristics of the perovskite solar cells without and with the treatment in ALD chamber, LHE spectrum of ALD-0 and ALD-5 solar cells, photovoltaic parameters of forward and backward for perovskite solar cells, photovoltaic performance of the cells with different thickness of absorberare included in the supplementary information. See DOI: 10.1039/b000000x/

1 C. R.Kagan, D. B.Mitzi, C. D.Dimitrakopoulos, *Science*, 1999, **286**, 945.
2 A. Kojima, M. Ikegami, K. Teshima, T.Miyasaka, *Chem. Lett.,* 2012, **41**, 397.
3 A.Kojima, K.Toshima, Y.Shirai, T.Miyasaka, *J. Am. Chem. Soc.,*2009, **131**, 6050.
4 H.-S.Kim, C.-R.Lee, J.-H.Im,K.-B.Lee, T.Moehl, A.Marchioro, S.-J.Moon, R.Humphry-Baker, J.-H.Yum, J. E.Moser, et al. *Sci. Rep.*,2012, **2**, 591.
5 J.Burschka, N.Pellet, S.-J.Moon, R.Humphry-Baker, P.Gao, M. K.Nazeeruddin, M.Grätzel, *Nature,*2013, **499**, 316.
6 K.Wojciechowski, M.Saliba, T.Leijtens, A.Abate, H. J. Snaith,*Energy Environ. Sci.,* 2014, **7**, 1142.
7 M. Liu, M. B. Johnston, H. J. Snaith, *Nature,* 2013, 501, 395-398.
8 H. Zhou, Q. Chen, G. Li, S. Luo, T. Song, H. -S. Duan, Z. Hong, J. You, Y. Liu, Y. Yang, *Science*2014, **345**, 542.
9 L.Etgar, P.Gao, Z.Xue, Q.Peng, A.K.Chandiran, B.Liu, M. K.Nazeeruddin,M.Grätzel, *J. Am. Chem. Soc.* 2012, **134**, 17396.
10 J.Shi, Y.Luo, H.Wei, J.Luo, J.Dong,S.Lv,J.Xiao, Y.Xu, L.Zhu, X.Xu, et al.*ACS Appl. Mater. Interfaces.* 2014, DOI: 10.1021/am502131t.
11 J.Shi, J.Dong, S.Lv, Y.Xu, L.Zhu,J.Xiao, X.Xu, H.Wu, D.Li, Y.Luo, et al. *Appl. Phys. Lett.* 2014, **104**, 063901.
12 S.Aharon, S.Gamliel, B. E.Cohen, L.Etgar, *Phys. Chem. Chem. Phys.* 2014, **16**, 10512.
13 A. Mei, X. Li, L. Liu, Z. Ku, T. Liu, Y. Rong, M. Xu, M. Hu, J. Chen, Y. Yang, M. Grätzel, H. Han, *Science*2014, **345**, 295.
14 Z. Wei, H. Chen, K. Yan, S. Yang, *Angew. Chemie Int. Ed.*DOI: 10.1002/anie.201408638.
15 J.Shi, W.Dong, Y. Xu, C.Li, S.Lv, L.Zhu, J.Dong, Y.Luo, D.Li, Q.Meng, et al. *Chin. Phys. Lett.* 2013, **12**, 128402.
16 Y.Xu, J.Shi, S.Lv, L.Zhu, J.Dong, H.Wu, Y.Xiao, Y.Luo, S.Wang, D.Li, X.Li, Q.Meng, *ACS Appl. Mater. Interfaces,*2014, **6**, 5651.
17 M. A.Green, A. W.Blakers, J.Shi, E. M.Keller, S. R.Wenham, *IEEE Trans. on Electron Devices* 1984, **31**, 671.
18 A.Abate, M.Saliba, D. J. Hollman, S. D.Stranks, K.Wojciechowski, R.Avolio, G.Grancini, A.Petrozza, H. J.Snaith, *Nano Lett.* 2014, DOI: 10.1021/nl500627x.
19 W. C.Wang, C. W.Lin, H. J.Chen, C. W.Chang, J. J.Huang, M. J.Yang, B.Tjahjono, J. J.Huang, W. C.Hsu, M. J. Chen,*ACS Appl. Mater. Interfaces,* 2013, **5**, 9752.
20 K. E.Roelofs, T. P.Brennan, J. C.Dominguez, C. D.Bailie, G. Y.Margulis,E. T.Hoke, M. D.McGehee, S. F.Bent, *J. Phys. Chem. C.* 2013, **117**, 5584.
21 P.Docampo, P.Tiwana, N.Sakai, H.Miura, L.Herz, T.Murakami, H. J.Snaith, *J. Phys. Chem. C.* 2012, **116**, 22840.
22 P. R.Brown, R. R.Lunt, N.Zhao, T. P.Osedach, D. D.Wanger, L.-Y.Chang, M. G.Bawendi, V.Bulovic, *Nano Lett.* 2011, **11**, 2955.
23 M. D.Groner, F. H.Fabreguette, J. W.Elam, S. M.George,*Chem. Mater.* 2004, **16**, 639.
24 C. A.Wilson, R. K.Grubbs, S. M. George,*Chem. Mater.* 2005, **17**, 5625.
25 X.Guo, Y. Luo, Y. Zhang, X. Huang, D. Li, Q. Meng,*Rev. Sci. Instrum.* 2010, **81**, 103106.
26 X. Guo, Y. Luo, C.Li, D.Qin, D. Li, Q. Meng,*Curr. Appl. Phys.* 2012, **12**, e54.
27 Thermo Fisher Scientific Inc. Thermo scientific XPS. http://xpssimplified.com/elements/aluminum.php.
28 A.Wagenpfahl, D.Rauh, M.Binder, C.Deibel, V.Dyakonov,*Phys. Rev. B.* 2010,**82**, 115306.
29 A.Dualeh, T.Moehl, N.Tétreault, J.Teuscher, P.Gao, K. N.Nazeeruddin, M.Grätzel, *ACS Nano* 2014, **8**, 362.
30 S. S.Hegedus, W. N.Shafarman, *Res. Appl.,* 2004, **12**, 155.
31 T.Fellmeth, M. J.Bartsch,D.Erath, U.Jäger,R.Preu, F.Clement, D. Brio,*IEEE Electron Dev. Lett.* 2011, **32**, 1101.
32 B.Vermang, V.Fjällström,X.Gao, M.Edoff, *IEEE J. Photovolt.* 2014, **4**, 486.
33 H.-S.Kim, I.Mora-Sero,V.Gonzalez-Pedro,F.Fabregat-Santiago,E. J.Juaez-Perez, N.-G.Park, J.Bisquert, *Nature Commun.* 2013, **4**, 2242.
34 A.Dualeh, T.Moehl, M. K.Nazeeruddin, M.Grätzel, *ACS Nano.* 2013, **7**, 2292.
35 V.Gonzalez-Pedro, E. J.Juarez-Perez, W.-S.Arsyad, E. M.Barea, F.Fabregat-Santiago, I.Mora-Sero, J.Bisquert, *Nano Lett.* 2014, **14**, 888.
36 J.Bisquert, L.Bertoluzzi, I.Mora-Sero, G.Garcia-Belmonte, *J. Phys. Chem. C.* 2014, **118**, 18983.
37 E. J.Juarez-Perez, M.Wuler, F.Fabregat-Santiago, K.Lakus-Wollny, E.Mankel, T.Mayer, W.Jaegermann, I.Mora-Sero, *J. Phys. Chem. Lett.* 2014, **5**, 680.
38 Sze, S. M.; Ng, K. K.; Physics of Semiconductor Devices, 3rd ed.; Wiley: New York, 2006.
39 M.A. Green, K. Emery, Y. Hishikawa, W.Warta, E.D. Dunlop, *Prog. Photovolt: Res. Appl.* 2013, **21**, 1.
40 X. B. Xiang, W.H. Du, X.L. Chang, H.R. Yuan, *Sol. Energ. Mat. Sol. C.* 2001, **68**, 97.
41 J. A.Christians,R. C. M.Fung, P. V. Kamat,*J. Am. Chem. Soc.* 2014, **136**, 758.